Progress toward an aberration-corrected low energy electron microscope for DNA sequencing and surface analysis

Marian Mankos[a] and Khashayar Shadman
Electron Optica Inc., 1000 Elwell Court #110, Palo Alto, California 94303

Alpha T. N'Diaye and Andreas K. Schmid
NCEM, Lawrence Berkeley National Laboratory, 1 Cyclotron Road, Berkeley, California 94720

Henrik H. J. Persson and Ronald W. Davis
Stanford Genome Technology Center, Stanford University School of Medicine, 855 California Avenue, Palo Alto, California 94304

(Received 27 June 2012; accepted 11 October 2012; published 26 October 2012)

Monochromatic, aberration-corrected, dual-beam low energy electron microscopy (MAD-LEEM) is a novel imaging technique aimed at high resolution imaging of macromolecules, nanoparticles, and surfaces. MAD-LEEM combines three innovative electron–optical concepts in a single tool: a monochromator, a mirror aberration corrector, and dual electron beam illumination. The monochromator reduces the energy spread of the illuminating electron beam, which significantly improves spectroscopic and spatial resolution. The aberration corrector is needed to achieve subnanometer resolution at landing energies of a few hundred electronvolts. The dual flood illumination approach eliminates charging effects generated when a conventional, single-beam LEEM is used to image insulating specimens. The low landing energy of electrons in the range of 0 to a few hundred electronvolts is also critical for avoiding radiation damage, as high energy electrons with kilo-electron-volt kinetic energies cause irreversible damage to many specimens, in particular biological molecules. The performance of the key electron–optical components of MAD-LEEM, the aberration corrector combined with the objective lens and a magnetic beam separator, was simulated. Initial results indicate that an electrostatic electron mirror has negative spherical and chromatic aberration coefficients that can be tuned over a large parameter range. The negative aberrations generated by the electron mirror can be used to compensate the aberrations of the LEEM objective lens for a range of electron energies and provide a path to achieving subnanometer spatial resolution. First experimental results on characterizing DNA molecules immobilized on Au substrates in a LEEM are presented. Images obtained in a spin-polarized LEEM demonstrate that high contrast is achievable at low electron energies in the range of 1–10 eV and show that small changes in landing energy have a strong impact on the achievable contrast. The MAD-LEEM approach promises to significantly improve the performance of a LEEM for a wide range of applications in the biosciences, material sciences, and nanotechnology where nanometer scale resolution and analytical capabilities are required. In particular, the microscope has the potential of delivering images of unlabeled DNA strands with nucleotide-specific contrast. This simplifies specimen preparation and significantly eases the computational complexity needed to assemble the DNA sequence from individual reads. © *2012 American Vacuum Society*. [http://dx.doi.org/10.1116/1.4764095]

I. INTRODUCTION

LEEM is a powerful parallel imaging technique pioneered in the 1980s by Bauer[1] and has been used extensively for the characterization of surfaces. The extremely low energy of the illuminating electrons makes LEEM an exquisitely sensitive surface imaging technique, capable of imaging single atomic layers with high contrast.[2] For example, Hibino[3] measured the electron reflectivity from thin graphite films formed on SiC(0001) and determined the graphite thickness from the quantized oscillation in the electron reflectivity. LEEM images of areas with a varying number of graphene layers, acquired over a range of landing energies, show oscillations in electron reflectivity that correspond to the number of graphene layers: the electron reflectivity data show that a layer composed of *m* graphene sheets produces m dips in the electron reflectivity spectra between 0 and 7 eV.

In the last decade, LEEM applications have been extended into semiconductor[4] and nanotechnology[5] applications. LEEM typically utilizes electron landing energies from 0 to few hundreds of electronvolts and images reflected rather than transmitted electrons. In Fig. 1, a schematic diagram of a typical TEM (left) and LEEM (right) are shown for comparison. The key difference in the LEEM column design is the departure from a straight optical axis column, necessitated by the need to separate the illuminating and scattered beams. In a LEEM, the illuminating electrons are emitted from the surface of a flat or pointed cathode, accelerated to the beam energy (10's of keV), and focused into a beam separator formed by a magnetic prism array. The beam

[a]Electronic mail:marian@electronoptica.com

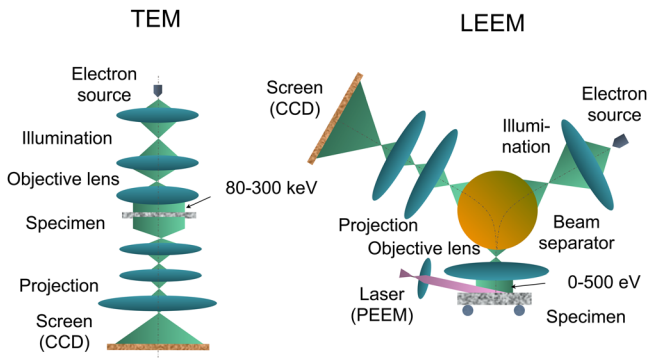

FIG. 1. (Color online) Schematic layout of a TEM and LEEM column.

separator deflects the electron beam from the illumination optics into the objective lens. The objective lens is an immersion cathode lens that decelerates electrons to a landing energy between 0 and a few 100 eV and illuminates the specimen surface with a broad beam. In the opposite direction, i.e., moving away from the specimen, the objective lens simultaneously accelerates the reflected and emitted electrons and forms a magnified image. The electrons reentering the beam separator are deflected into the projection optics, which magnifies the image on a scintillating screen. The image formed on the screen is then viewed by a CCD camera and saved on a computer.

The main drawbacks of LEEM are its lateral resolution and charging effects. In spite of the short deBroglie wavelength, which is in the Angstrom range, the lateral resolution of conventional LEEM instruments is limited to 4–5 nm at a landing energy of 10 eV, and subnanometer resolution has not been achieved yet. In addition, when a conventional LEEM is used to image insulating specimens, the low landing energy exacerbates charging effects resulting in reduced image quality.

II. ELECTRON OPTICS

A schematic layout of the MAD-LEEM electron–optical column, combining two independent illumination beams with a monochromator and an aberration corrector, is shown in Fig. 2. The illumination optics has two branches, one for an imaging beam (solid, orange lines) and one for a charge control mirror beam (short dash, green lines), which are combined by the main beam separator. The imaging beam illumination optics includes a monochromator that reduces the electron energy spread to less than 0.1 eV. The main beam separator deflects both beams toward the lower beam separator, which transports the beam into the objective lens, where the electrons are decelerated and focused to form parallel flood beams. The imaging beam has a landing energy of up to several 100 eV, and the charge control mirror beam has a landing energy near 0 eV. The electrons are backscattered by the specimen, reaccelerated, and focused by the objective lens to form a two-dimensional, aberrated image. The lower beam separator deflects the image formed by backscattered electrons first into a symmetry mirror that compensates for the energy dispersion of the beam separator and then into a

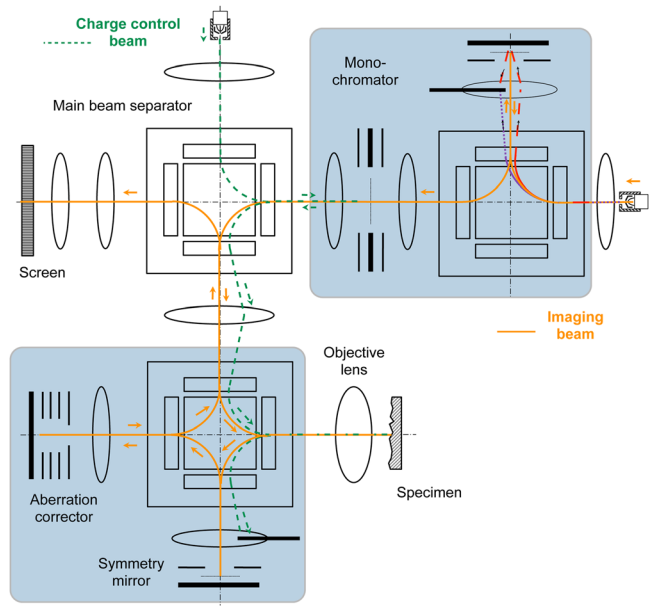

FIG. 2. (Color online) Electron–optical diagram of the MAD-LEEM column.

mirror aberration corrector (MAC) that corrects the spherical and chromatic aberrations of the objective lens. The symmetry mirror reflects a highly magnified image, which minimizes the aberration contribution of the symmetry mirror. Rotation-free magnetic doublet lenses are utilized to transfer the image between the beam separator and the electron mirror in order to avoid rotation of the chromatic dispersion plane. Residual aberrations due to the symmetry mirror and transfer lenses can be corrected by the MAC. The mirrored electrons that were not absorbed as well as any secondary electrons generated by the specimen can be stopped by a knife edge aperture so as to not blur the image formed by the backscattered imaging beam. Electrons returned by the aberration corrector are then deflected by the lower beam separator back toward the main beam separator. Finally, the electrons are transported into the projection optics that magnifies the image on a scintillating screen.

A. Monochromator

The energy spread of electron sources used commonly in electron microscopy, which comprise thermionic (W, LaB_6) and thermally assisted (Schottky, ZrO_2) field emission cathodes, is in the range of 0.5 to 2 eV. In order to obtain detailed information about the chemical composition of a surface, interatomic bonding and local electronic states of macromolecules and nanoparticles, as well as defects and other aperiodic objects, an energy resolution of 0.1 eV or less is necessary.[6,7] Although multiple monochromator designs have been proposed and realized,[6,8] a LEEM equipped with an electron mirror lends itself to a novel design,[9] as shown in Fig. 3. The electron source, biased at a high negative voltage, emits electrons with an energy spread, ΔE. After the illumination zoom optics, the beam passes through a beam separator, which deflects the beam into an electron mirror. The electrons with nominal beam energy E_0 (solid, green

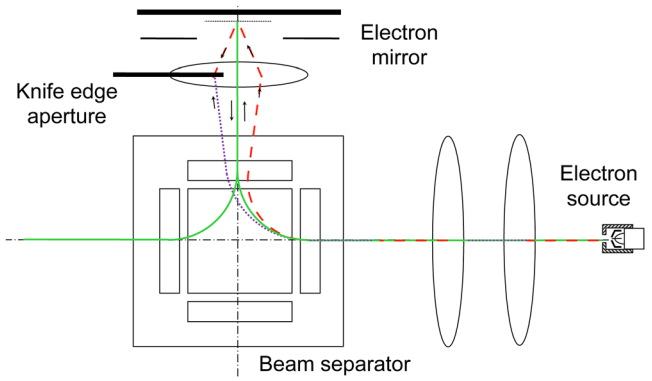

FIG. 3. (Color online) Electron–optical diagram of monochromator with magnetic prism separator and electron mirror.

lines) are deflected by 90°, while electrons with a slightly lower energy (dashed red lines) or higher energy (dotted, purple lines) are deflected slightly more or less, respectively, as a result of the energy dispersion of the beam separator. The axial bundle of rays with energies in the range ($E_0 - \Delta E$, $E_0 + \Delta E$) appears to emanate from a point near the center plane of the beam separator, also known as the achromatic point (plane). As the electrons proceed toward the electron mirror, a knife edge-shaped aperture stops the electrons with slightly higher energies, $E_0 + \Delta E$, as shown in Fig. 3. The transfer lens focuses the achromatic point at the reflection plane of the electron mirror, which is biased slightly more negative than the electron source, and thus reflects all the electrons back into the beam separator. As the remaining electrons proceed back to the beam separator, the lower energy electrons with energies $E_0 - \Delta E$ are stopped by the same knife edge-shaped aperture. This arrangement allows the use of a simple knife edge as the energy selecting device, which is a much simpler and more reliable design when compared to the narrow, often submicron slits needed in typical monochromator designs. The remaining electrons have an energy spread that is less than 100 meV. These electrons re-enter the beam separator and are deflected once again by 90° onto the axis of the electron source. After the double pass through the beam separator and the electron mirror, the dispersion introduced by the monochromator vanishes due to symmetry, which is desirable for high resolution imaging.

In principle, a single pass through the 90° beam separator provides the dispersion needed to monochromatize the beam with a slit aperture. However, without the second pass through the beam separator, the beam would acquire energy dispersion, which is detrimental for high resolution imaging in the remaining optics as cross-term aberrations between the dispersion and lens aberrations cannot be corrected by the aberration corrector. The added reflection in the electron mirror implies that additional electromagnetic deflectors are needed to accurately position the beam with respect to the energy-selective knife-edge aperture.

This novel monochromator design has also the potential to further improve the spatial resolution of a LEEM, as it reduces the higher order chromatic aberrations, thereby easing the task for the aberration corrector. With minimized higher chromatic aberrations, the aberration corrector can then be used to remove the remaining 5th order spherical aberration. In addition, the monochromator together with an electron gun can be used as a stand-alone unit[10] to provide a source of monochromatic electrons that can be utilized to significantly improve spatial resolution in low-voltage SEM (LVSEM) and improve energy resolution and spectroscopy in energy-filtered TEM.

B. Aberration corrector

The best lateral resolution that has been achieved in practice in a LEEM without aberration correction is between 4 and 5 nm at 10 eV landing energy, and ~10 nm at 1 eV. Due to the low electron energies used in a LEEM, the resolution is limited by diffraction and chromatic and spherical aberrations of the objective lens. At very low electron energies, the resolution is dominated by diffraction due to the inverse square root relationship between wavelength and energy: at 1 eV, the electron deBroglie wavelength is 1.2 nm. At an electron energy of 150 eV, the wavelength falls to 0.1 nm, and chromatic and spherical aberrations of the objective lens determine the resolution. Although the incorporation of the monochromator reduces the chromatic aberration significantly, it does not sufficiently improve the resolution into the subnanometer regime, making an aberration corrector a necessity.[2,7] Scherzer[11] in 1936 established that chromatic and spherical aberrations of static round lenses are unavoidable in the absence of space charge and flight reversal. Since then, multiple paths to aberration correction have been pursued, including multipole lenses,[12,13] time-dependent fields, charged foils, and grids as well as electron mirrors.[14] A LEEM already includes a path reversal in the objective lens, so the MAC is a natural choice. Recent experimental results[15,16] with aberration correction in LEEM have demonstrated the principle by improving the lateral resolution to 2–3 nm.

In an aberration-corrected LEEM, the spatial resolution can be improved by eliminating one or more aberrations of the objective lens. Schmidt *et al.*[15] and Tromp *et al.*[16] utilized a tetrode MAC (Ref. 17) that eliminates both the chromatic and spherical aberration of the objective lens to improve the spatial resolution. Conventional rotationally symmetric electron lenses strongly focus electron rays with larger entrance slopes and lower energies, resulting in positive spherical and chromatic aberration coefficients. Electron mirrors, on the other hand, can be adjusted to weakly focus the aforementioned rays, thus yielding negative spherical and chromatic aberration coefficients. As pointed out by Schmidt,[18] once the primary spherical and chromatic aberrations are eliminated by the MAC, the resolution is determined by diffraction and higher rank chromatic and 5th order geometric aberrations.

The electron–optical properties of the objective lens ultimately limit the resolution attainable in a LEEM. The specimen is biased at a high negative voltage (tens of kilovolt) and is thereby immersed in a high electrostatic field. This field when combined with the effect of the objective lens

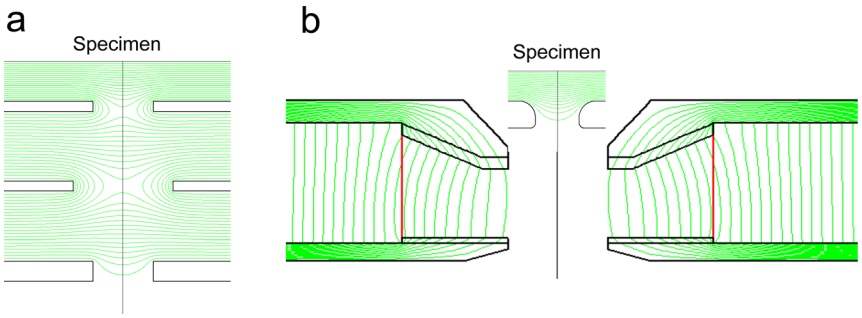

FIG. 4. (Color online) Geometry, and equipotential and flux density distributions of typical LEEM objective lenses: (a) electrostatic and (b) magnetic.

produces a magnified virtual image of the specimen surface.[19] Two types of objective lenses were considered: electrostatic and magnetic lenses. The geometry of the individual lenses is shown in Fig. 4. Both objective lenses have an accelerating field of approximately 5 kV/mm at the specimen surface and produce a beam energy of 20 kV. The geometry of the focusing electrodes and polepieces was chosen to give a practical lens design capable of forming a magnified image of reasonable size (few tens of micrometer) at a distance of 260 mm from the substrate. The electrode and polepiece geometry utilizes designs optimized for LEEM/PEEM. The equipotential distribution of the electrostatic fields and of the flux density is also shown in Fig. 4. The objective lens used in our simulations has been modified for a reduced electric field of 5 kV/mm at the surface in order to minimize arcing during operation. The field is about a factor of two lower than the objective lens considered by Tromp.[20] The lower electric field increases the focal length of the magnetic lens, which increases the spherical aberration. In addition, the magnetic lens is designed to produce a negligible magnetic field at the substrate in order to minimize aberrations in the diffraction plane. The vanishing magnetic field also increases the focal length of the lens and thereby the spherical aberration. The larger spherical aberration of this lens, however, can be eliminated by the aberration corrector. However, it is duly noted that an objective lens designed with higher field strength may have some advantages and will be considered in the final design.

The specialized software package MIRROR DA (Ref. 21) developed by MEBS, Ltd., has been used for the aberration analysis of the objective lenses and of the electron mirrors that are used for aberration correction. The differential algebra-based (DA) software package computes aberrations of any order electron mirrors with any symmetry and can handle combinations of electron mirrors and electron lenses in a unified way. Results computed with MIRROR DA were shown to be in good agreement with those extracted by direct ray tracing with relative deviations of less than 0.065% for all primary aberration coefficients.[21] Table I shows the computed values of the key aberration coefficients (referred to the image plane) for an 1 eV electron energy of 1 eV obtained by MIRROR DA for both types of objective lenses with the image plane at a distance of 260 mm from the substrate surface. As the aberration coefficients of the purely electrostatic lens are substantially larger when compared to the magnetic objective lens, the following analysis pertains exclusively to the magnetic objective lens. Simulations of electron–optical properties of the magnetic objective lens have been completed for aberrations up to 5th order in order to understand the resolution limit with aberration correction. The result of this analysis for an electron energy of 1 eV with an initial energy spread of 0.25 eV and a field of view of 2 μm on the specimen is shown in Fig. 5. This figure shows a plot of all aberrations up to 5th order that are larger than 0.1 nm as a function of the emission angle. The 3rd order geometric and (2nd rank) chromatic aberrations are drawn in dashed lines, while 5th order aberrations are drawn in dotted lines. The total resolution is then obtained by adding all terms using Gaussian quadrature. Without aberration correction, the resolution is limited by the spherical, chromatic, and diffraction aberrations to approximately 8 nm at 1 eV electron energy.

In the next step, the tetrode MAC refined by Wan *et al.*[22] and Tromp *et al.*[16] was analyzed. This MAC, shown in Fig. 6, consists of four electrodes: a mirror electrode maintained at a potential more negative than the electron source,

TABLE I. Electron-optical properties of objective lenses with aberration correction at 1 eV electron energy.

	Electron–optical element			
Parameter	Electrostatic objective	Magnetic objective	Tetrode corrector	Magnetic objective + tetrode corrector
Magnification	10.02	9.49	1.00	9.49
Third order spherical aberration coeff. [m]	28 337	−14 279	−14 286	−7
Second rank chromatic aberration coeff. [m]	81.27	52.59	−52.65	−0.06
Fifth order spherical aberration coeff. [m]	-8.173×10^{10}	-3.638×10^{10}	-7.175×10^{7}	-3.645×10^{10}
Third rank chromatic aberration coeff. [m]	−487 553	−275 505	200.2	−275 304.8
Fourth rank chromatic aberration coeff. [m]	8.633×10^{8}	4.294×10^{8}	1.247×10^{5}	4.295×10^{8}

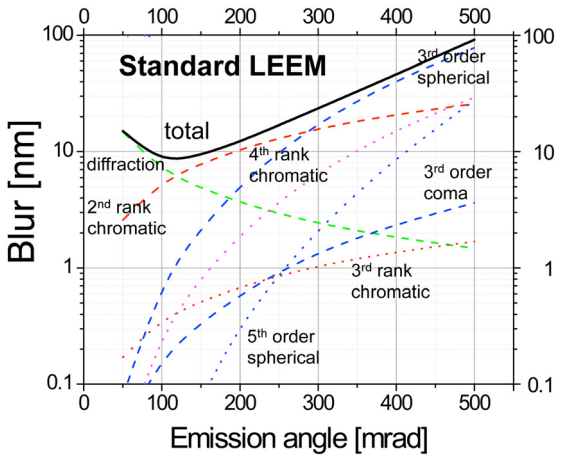

FIG. 5. (Color online) Magnetic objective lens aberrations for a range of electron emission angles.

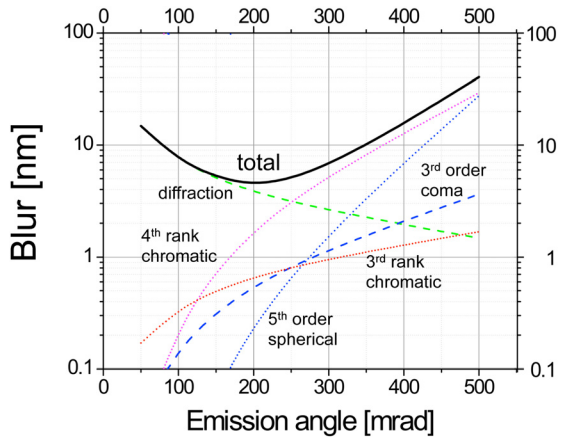

FIG. 7. (Color online) Magnetic objective lens aberrations with correction of primary spherical and chromatic aberrations for a range of electron emission angles.

two intermediate aperture electrodes, and a ground electrode. The latter three electrodes have a bore diameter of 8 mm. The potential of the mirror as well as the two intermediate electrodes can be varied to independently set the focus and simultaneously adjust the primary spherical (C_s) and chromatic (C_c) aberration coefficients of the tetrode MAC. The focus of the MAC is set to produce a 1× magnified image at the object plane at a distance of 240 mm from the mirror electrode. Once the focus is set, the tetrode MAC spherical and chromatic aberration coefficients are fine-tuned iteratively to cancel aberrations of the combined magnetic objective lens: the tetrode MAC corrects the primary spherical and chromatic aberrations of the cathode objective lens at 1 eV electron energy to 0.1% or better, as illustrated in Table I. With the aberration corrector switched on and the electrode potentials set to the values shown in Fig. 6, the resolution is now limited by diffraction, 3rd and 4th rank chromatic and 5th order spherical aberrations to approximately 4.5 nm at 1 eV electron energy, as shown in Fig. 7.

In the MAD-LEEM approach, the built-in monochromator lowers the energy spread of the illuminating electrons by a factor of 10 to 25 meV, which further reduces the higher rank chromatic aberrations, in particular at low landing energies. This reduces the blur further to approximately 3 nm, and diffraction and 5th order spherical aberration become the dominant aberrations, as shown in Fig. 8.

The reduction of the higher rank chromatic aberrations is rather important, in particular in the case of an objective lens with larger spherical aberrations. With the higher chromatic aberrations minimized by the monochromator, it is in principle possible to further improve the resolution[23] by correcting the dominant 5th order spherical aberration by replacing the tetrode MAC with a novel aberration corrector, a pentode MAC. A pentode MAC includes one additional electrode, which provides the needed degree of freedom to correct one additional aberration. Work is currently in progress to optimize the pentode MAC, and it is anticipated that this will improve the resolution to approximately 2.5 nm at 1 eV landing energy. With the pentode MAC, diffraction and the residual 4th rank chromatic aberration are then the remaining aberrations, as shown in Fig. 9.

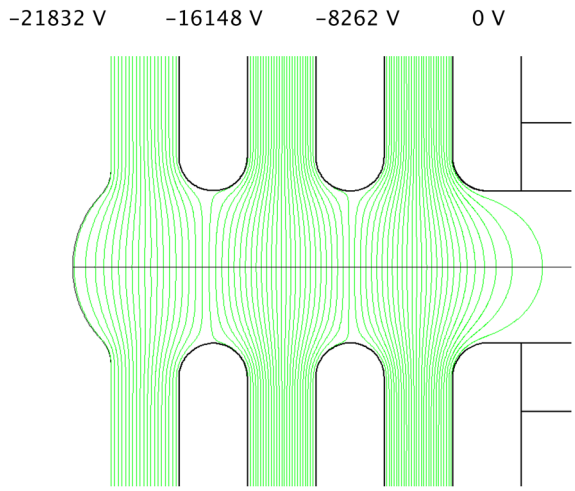

FIG. 6. (Color online) Geometry and equipotential distribution of a tetrode MAC.

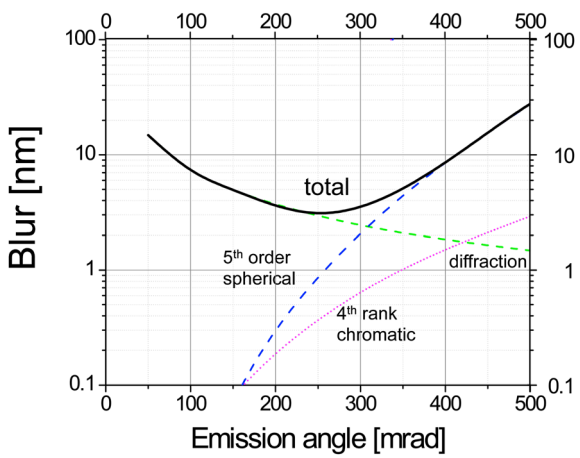

FIG. 8. (Color online) Magnetic objective lens aberrations with correction of primary spherical and chromatic aberrations and monochromator for a range of electron emission angles.

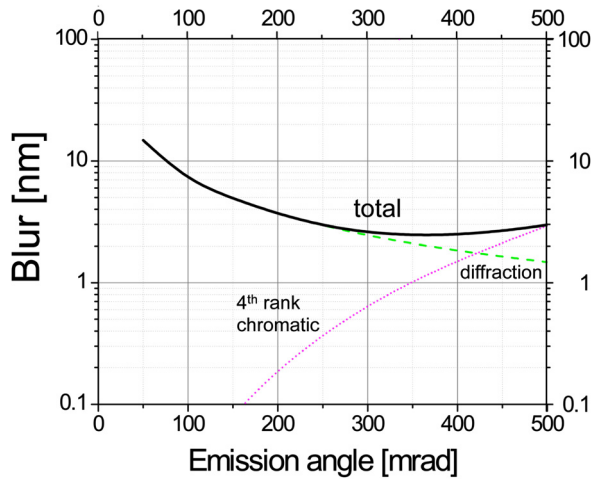

FIG. 9. (Color online) Magnetic objective lens aberrations with correction of 3rd and 5th order spherical and primary chromatic aberrations and 25 meV monochromaticity for a range of electron emission angles.

Further significant improvement in resolution is then achievable only by reducing the diffraction aberration, which can be accomplished by increasing the landing energy of the electrons to 100–200 eV (compared to 5–10 eV used by Schmidt *et al.*[15] and Tromp *et al.*[16]). We have repeated the aberration analysis for higher energies in a similar fashion to the previously illustrated 1 eV example, and the summary is shown in Fig. 10. It can be seen that with the tetrode MAC, the resolution approaches 1 nm at 200 eV and in principle can be extended into the subnanometer regime with a pentode MAC. With a pentode MAC, the blur falls below 1 nm at 30 eV landing energy and drops to approximately 0.7 nm at 100 eV.

C. Dual beam illumination

The MAD-LEEM features a dual beam approach that eliminates the risk of charging the specimen by illuminating

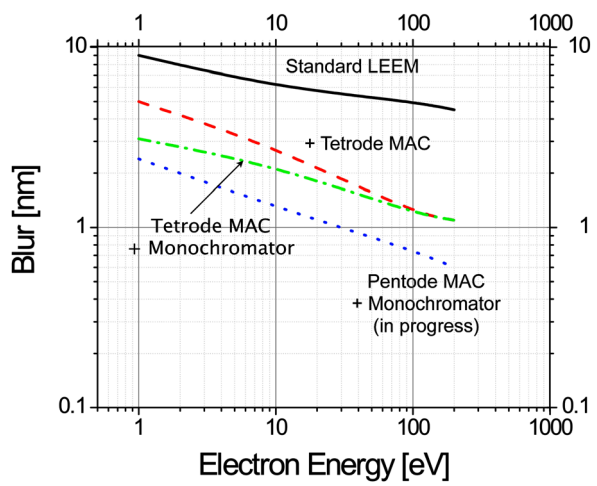

FIG. 10. (Color online) Minimum blur achievable in a LEEM as a function of electron energy for different aberration correction schemes: conventional LEEM (solid, black line), LEEM with tetrode MAC (red, dashed line), LEEM with tetrode MAC and monochromator (dotted–dashed, green line) and LEEM with pentode MAC (dotted, blue line).

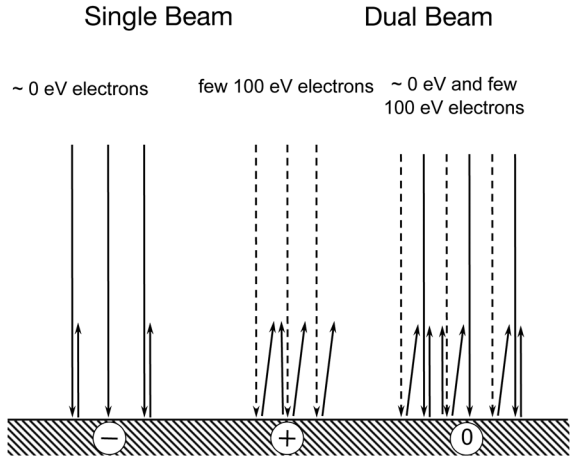

FIG. 11. Surface charging with single beam and charge balance under dual beam illumination.

it with two superimposed flood beams with opposing effects. In a dual-beam LEEM, originally proposed in the early 1990s by Veneklasen, two electron beams with different landing energies are used to mitigate the charging effect (Fig. 11). When an insulating specimen is illuminated with a low energy mirror electron beam with landing energy near 0 eV, a fraction of the electrons is mirrored and the remainder is absorbed, charging the surface negatively. When a higher energy electron beam (few 100 eV) is used, secondary electrons are emitted, and the electron yield can exceed 1, charging the surface positively. However, when these two electron beams are superimposed on the substrate, charging effects can be neutralized. Multiple electron–optical implementations of a LEEM with dual-beam illumination have been proposed and developed.[23–26] Several dual-beam LEEM prototypes have been successfully designed and built and the dual-beam charge control approach has been demonstrated experimentally on a variety of samples, including oxide structures on Si, resist-coated wafers, and quartz imprint masks.[24] The challenge is to devise an electron–optical design that fits into the system layout and can deliver overlapping illumination of the charge control mirror and imaging electron beams at preferably normal incidence on the specimen, in a other words, a system that combines two parallel electron beams with different energies and beam currents at the specimen surface.

The illumination configuration shown in Fig. 2 includes two perpendicular branches, which are joined by the main magnetic beam separator. The first, vertical branch includes an electron gun that generates the charge control mirror beam with a lower potential energy U. The charge control mirror beam is deflected by the main beam separator by 90° into the horizontal axis and enters an electrostatic einzel lens configured as an electron mirror, where the center electrode is biased slightly more negative than the first electron gun to reflect the mirror beam back toward the main beam separator.

The second electron gun, biased more negatively than the mirror einzel lens, generates the imaging beam, which passes through the mirror einzel lens and into the main beam

separator. The imaging beam is deflected by the main beam separator by 90°, while the mirror beam is deflected by slightly more than 90°, typically a fraction of a degree to a few degrees, due to the energy dispersion of the main beam separator. In order to compensate for this and assure that the two beams are coaxial when they pass through the objective lens and illuminate the specimen, the mirror beam is focused by a field lens that couples the main beam separator to the lower beam separator.

The presence of three beam separators in the column increases the complexity of the optics and necessitates the addition of properly positioned and dimensioned alignment elements. Previous implementations[4,26] of LEEM columns with multiple magnetic prism array-based beam separators have demonstrated that the design, fabrication and test is a manageable (albeit complex) task resulting in stable and reliable column performance.

III. APPLICATION: DNA SEQUENCING

Deoxyribonucleic acid, or DNA, is a nucleic acid that harbors the genetic information needed for the development and functioning of living organisms. DNA consists of two long polymer strands, entwined like vines in the shape of a double helix.[27] The backbone of the strand is made of sugars and phosphate groups, and attached to each sugar is one of four types of molecules called bases: adenine (A), cytosine (C), guanine (G), and thymine (T). It is the sequence of these four bases along the backbone that encodes the genetic information. In a DNA double helix, the bases form complementary base pairs: A forms a base pair with T and G forms a base pair with C. The base pairs are bonded by relatively weak hydrogen bonds, and thus, the two strands of DNA in a double helix can be pulled apart like a zipper, not only by enzymes but also by a mechanical force or high temperature. As a result of the complementary base pairing, all the information in the double-stranded sequence of a DNA (ds-DNA) helix is duplicated on each strand. This means that one can in principle image either the double helix or a single strand (ss-DNA) for DNA sequencing.

Significant demand exists for the development of novel technologies capable of low-cost, high quality DNA sequencing. Established sequencing techniques based on capillary array electrophoresis and cyclic array sequencing offer such analytical capability, and next generation, high throughput commercial sequencers deliver at a cost approaching $10,000/genome. One drawback is that these technologies identify in one segment (read) only about 10–1000 sequential base pairs out of the total 3×10^9 base pairs in the human genome. The complex repetitive nature of DNA makes it costly and time consuming to completely and accurately reassemble a full genome.

Recently, transmission electron microscopy (TEM) techniques[28,29] have been proposed that label specific DNA bases with heavy atoms (e.g., osmium) and thus have the promise of significantly extending the length of individual reads. However, the accurate determination of the complete DNA sequence is complicated by the need for labeling and correlating the labeled and unlabeled bases. In addition, the relatively high electron energy used in high resolution TEMs causes radiation damage that leads to read errors and limits the usable electron dose. The MAD-LEEM approach has several key advantages when compared to these TEM techniques: low electron landing energy, potential for label-free nucleotide specific contrast, and charge control.

The low landing energy of electrons in a LEEM is critical for avoiding radiation damage and achieving high exposure doses, as high energy (>1 keV) electrons cause irreversible damage to biological molecules. Experimental work carried out by Fink's group[30] suggests that DNA withstands electron radiation with electron energies in the range from 60 to 230 eV, despite a vast dose of 10^8 electrons/nm^2 accumulated over more than one hour. A high electron dose is critical for achieving high throughput, as throughput scales directly with electron dose.

In the MAD-LEEM design, a monochromator is introduced into the illumination optics, which is key to probing and differentiating the electronic states of individual nucleotides. Theoretical studies[31] using density functional theory computations of the internal electronic structure of single DNA bases adsorbed on a Cu(111) surface show a diversity of geometrical and electronic structures for each of the individual nucleotides that can result in different electron reflectivity spectra analogous to Hibino's approach[3] for determining the graphite thickness. The characteristic signature imprinted in the reflectivity spectra has the potential to distinguish the individual unlabeled bases and lead to image contrast that can be utilized to determine the sequence of nucleotides in a DNA strand. The MAD-LEEM approach with monochromatic, low energy illumination is ideally suited to deliver the resolution and to achieve the necessary contrast given that the energy levels are expected to vary on the order of a fraction of 1 eV.

The conductivity of DNA is claimed to vary from that of an insulator to that of a superconductor,[32,33] depending on the substrate and the way DNA is attached to the electrodes. When a partially or fully insulating macromolecule is imaged with an electron beam, the imbalance between the arriving and leaving electron flux may cause the macromolecule to charge, resulting in added blur. The MAD-LEEM design incorporates a charge control mirror beam that prevents the charging of individual molecules. In case the individual DNA strands are sufficiently conductive to prevent charging, the mirror beam can be turned off.

The complete human genome holds about 3×10^9 base pairs spaced 0.34 nm apart and is approximately 1.5 m long when fully stretched out on a substrate. It is anticipated that a technology that can sequence the genome at a target cost of about $1,000 has the ability to generate routinely complete genomic sequences that would revolutionize biological research and make comprehensive genomic sequence information available for individual health care. In order to meet a desired $1000/genome cost target, a throughput commensurate with reading one complete genome in 12 h or less or 250×10^6 base pairs per hour are needed. A DNA sequencing

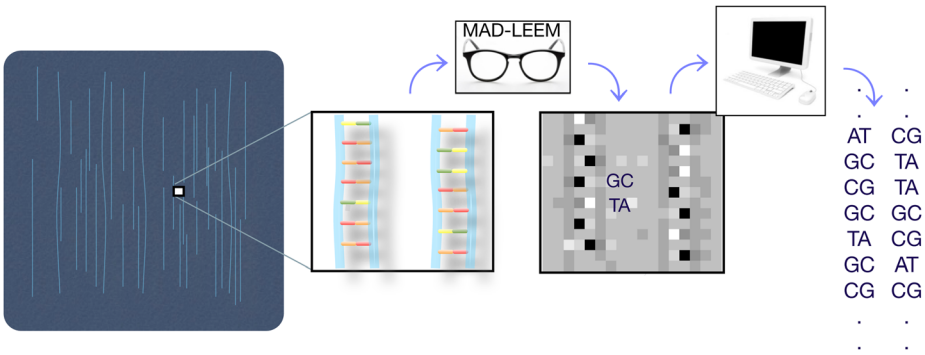

FIG. 12. (Color online) Sequencing strategy using a MAD-LEEM, from left to right: substrate with stretched out DNA strands, magnified view of sections of two DNA strands, anticipated nucleotide-specific contrast, identified DNA base sequence.

strategy that is aimed at achieving this throughput is outlined in Fig. 12.

First, a substrate with densely packed, stretched out strands of DNA is prepared, by using molecular combing[34] techniques. Molecular combing attaches an array of single DNA molecules with a random-coil configuration to a silanised substrate by their extremities. When the substrate is slowly removed from the solution, DNA molecules are uniformly stretched and aligned by the receding air–water meniscus and adhere to the substrate along their length, thus preventing retraction. Arrays of thousands of combed molecules as long as 5×10^6 base pairs with increased base spacing (from 0.34 to 0.5 nm for ds-DNA and 0.7 nm for ss-DNA) can be prepared with this method.

In the next step, the substrate with the attached DNA molecules is inserted into the microscope and imaging conditions yielding nucleotide-specific contrast are obtained by tuning the landing energy. For ds-DNA, the task is reduced to distinguishing the two base pairs (AT and GC) and determining their orientation (AT or TA and GC or CG). This reduces the image resolution requirements as we seek only to distinguish two molecule pairs from each other and do not require the imaging of individual atoms. For imaging of ss-DNA, each of the four bases needs to be distinguished with a 0.7 nm pitch.

In the final step, the acquired gray-level image is analyzed on-the-fly by an image computer. Images of individual bases or pairs are located and correlated with the anticipated contrast, and the base sequence is determined for each DNA strand in the field of view and stored in the computer memory.

IV. EXPERIMENT

The goal of the experimental work is to establish that electron reflectivity at low electron energies in the 1–200 eV range is sensitive enough to distinguish individual nucleotides or pairs. In order to get some insight in the achievable contrast, we are aiming to obtain experimental contrast values from bulk single base (A,C, G, or T) DNA structures, which can be obtained at lower resolution. We hypothesize that this contrast will prevail for the individual bases at high resolution as well.

Low energy electron scattering is directly related to the sample's electronic structure, and because different nucleotides have different electronic structure, the electron scattering coefficients should be nucleotide dependent. This can result in observable contrast, provided the differences between the individual scattering coefficients are large enough. As there is currently no LEEM capable of imaging DNA with resolution needed to distinguish the individual bases, the imaging and acquisition of electron reflectivity spectra was performed on relatively large DNA samples synthesized with one base type only, thus circumventing the high resolution requirement. The experimental results presented in the following sections are still preliminary. We have included the experimental results in this paper, as the experimental contrast obtained from DNA in a LEEM is novel and shows that this technique may be feasible.

The experimental work described in this paper has been performed at the Stanford Genome Technology Center, Stanford University in Palo Alto, CA and at the LBNL National Center for Electron Microscopy in Berkeley, CA.

A. Sample preparation and characterization

A variety of samples with one type of base (oligonucleotides) supplied by Integrated DNA Technologies was prepared for detailed characterization, including both ss-DNA and ds-DNA. For ss-DNA, 100 bases long A and C oligonucleotides and 200 bases long T oligonucleotides, as well as shorter, 20 bases long G and T oligonucleotides were used. In addition, dithiol-modified oligonucleotides (5′-/5DTPA/A-20mer, 5′-/5DTPA/C-20mer) were utilized in order to improve the adhesion to gold substrates. For ds-DNA specimens, the short oligonucleotides (G-20mers) were hybridized with the dithiol-modified oligonucleotides (5′-/5DTPA/C-20mers).

All the samples were prepared on mica peeled gold on glass substrates manufactured by Nanoink[35] Inc., which provide a fresh, clean, atomically flat gold surface for DNA deposition. The gold surface remains in contact with the mica until deposition, when a fresh gold substrate free of contaminants is created by separating the gold from the mica. Conductive and smooth substrates with minimum roughness are ideal for LEEM imaging of molecules attached on surfaces. We have imaged clean mica peeled gold on glass substrates and found good correlation between AFM and LEEM (Fig. 13) imaging results, confirming the subnanometer local roughness.

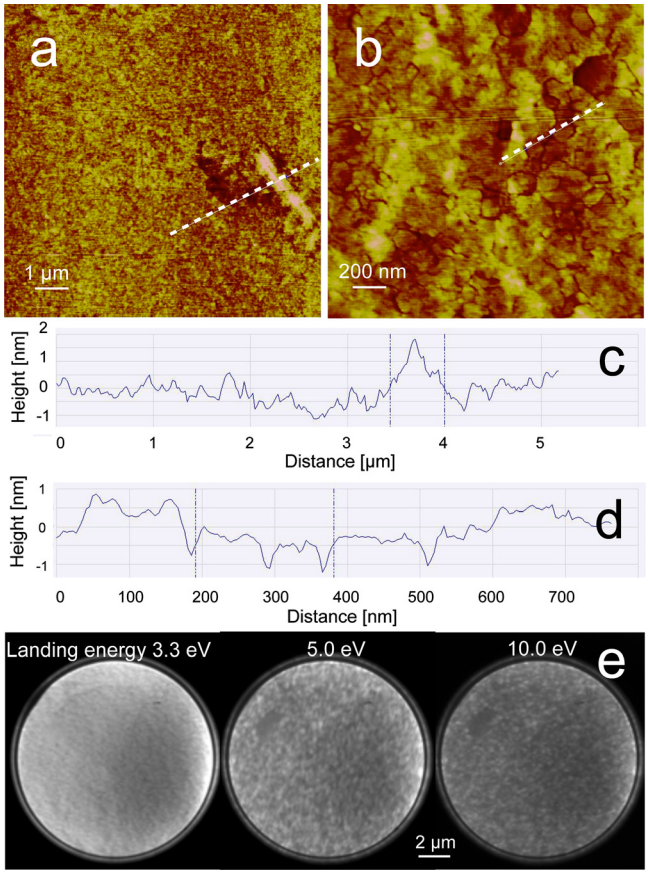

FIG. 13. (Color online) Imaging of clean Au substrates: (a), (b) AFM images at two magnifications, (c) height profile along line shown in (a), (d) height profile along line shown in (b), (e) LEEM images at three different landing energies.

All oligonucleotides were dissolved in $1 \times$ TE buffer (10 mM Tris-HCl, 1 mM EDTA, *p*H 8.0) and diluted to 10 μM concentration. Oligonucleotide solutions of 25–60 μl were spotted onto freshly cleaved gold substrates and incubated for 16 h in the dark under controlled humidity. Spotted gold substrates were washed with a 2 ml $0.1 \times$ TE buffer and dried in air except for long unmodified oligonucleotides and prehybridized ds-DNA where the rinsing step was omitted. Reduction of dithiol-modified oligonucleotides was accomplished using a 40-fold excess of Tris(2-carboxyethyl)phosphine hydrochloride (TCEP–HCl) for 2 h at room temperature followed by purification using a spin column (Pall Nanosep, MWCO = 3000). Double-stranded DNA synthesis was accomplished by mixing reduced dithiol-C20mer with a 2-fold excess of G20mer, heating to 95 °C followed by cooling to room temperature prior to immobilization.

B. LEEM imaging

The spin-polarized low-energy electron microscope (SPLEEM) at LBNL was used to investigate the contrast achievable in a LEEM on samples of unlabeled sections of ss-DNA with solely A, C, G, and T oligonucleotides and selected ds-DNA molecules. The SPLEEM at NCEM has a spatial resolution in the range of 10 nm and is therefore not capable of imaging individual DNA bases, but it is well suited for imaging thin layers or islands of DNA on a flat surface provided no surface charging occurs. The spin-polarized electron source produces a very low energy spread of ~100 meV. It also has the capability of producing landing energies in the range of 0 eV to a few 100 eV, which is ideal for the imaging and spectroscopy of biological materials.

The imaging of the various preparations of the DNA samples showed that the reduced dithiol-modified oligonucleotides held the most promise. These oligonucleotides formed small islands on the Au surface, which are suitable for spectroscopic measurements of electron reflectivity. Un-reduced dithiol-modified oligonucleotides formed fractal-like structures, which were not suitable for our spectroscopy measurements. Examples of LEEM images of both reduced and unreduced dithiol-modified oligonucleotides deposited on Au substrates (Fig. 14) show that high contrast is indeed achievable at very low electron landing energy. A qualitative comparison of the LEEM results (Fig. 15, bottom) to that of an AFM (Fig. 15, top) confirms the topography of the islands formed by attachment of single-DNA base oligomers on Au substrates. On the other hand, long ss-DNA oligomers and hybridized ds-DNA structures charged up severely under electron illumination in the LEEM, likely due to the missing salt rinse step and consequent presence of salt crystals.

C. Electron reflectivity measurements

Electron reflectivity measurements (Fig. 16) were performed in the SPLEEM over a range of landing energies. Image series of reduced dithiol-modified oligonucleotides at

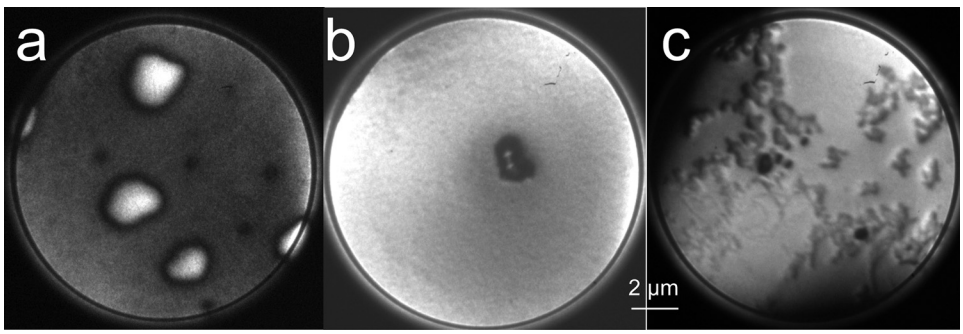

FIG. 14. LEEM images of dithiol-modified oligomers deposited on Au substrates: (a) reduced 5′-/5DTPA/C-20mer at 2.9 eV landing energy, (b) reduced 5′-/5DTPA/A-20mer at 3.1 eV landing energy, and (c) unreduced 5′-/5DTPA/C-20mer at 4.3 eV landing energy. Field of view is 13 μm.

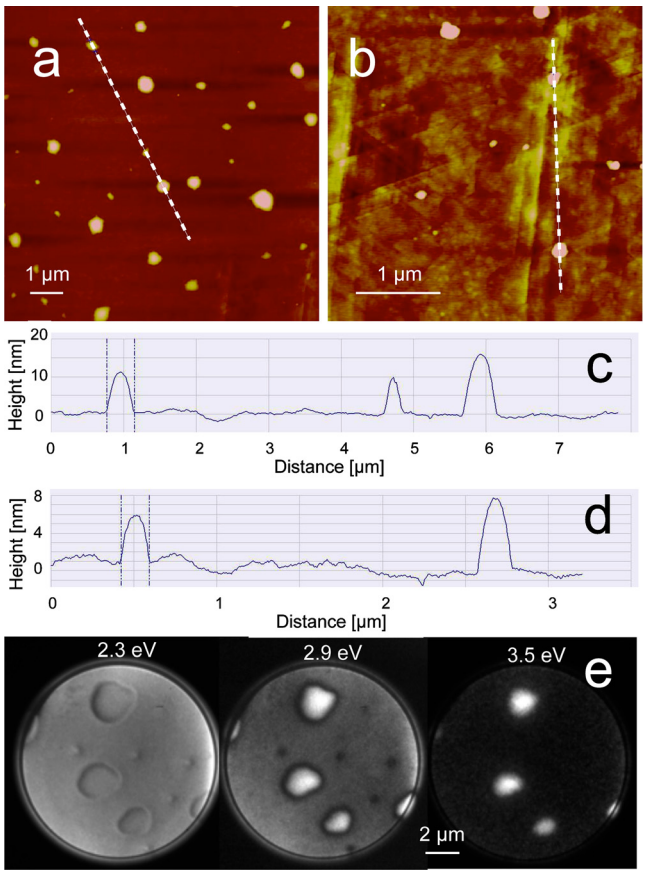

FIG. 15. (Color online) Imaging of reduced 5′-/5DTPA/C-20mer on Au substrate: (a) (b) AFM images at two magnifications, (c) height profile along line shown in (a), (d) height profile along line shown in (b), and (e) LEEM images at three different landing energies.

varying electron landing energy demonstrate the high contrast achievable at low electron energies: deposited DNA structures are easily visible over a range of landing energies. They also show that small changes in landing energy have a strong impact on the achievable contrast.

First, electron reflectivity spectra from freshly cleaved Au substrates without any immobilized DNA were acquired in the SPLEEM over a range of landing energies from 0 to 20 eV (Fig. 16, top). The reflectivity data were derived by averaging the intensity over a square, $1\,\mu m \times 1\,\mu m$ area while the landing energy is increased in 0.1 eV steps. The electron reflectivity spectra, acquired at three different locations across the substrate surface, show peaks at 4 and 8 eV landing energy, which provide a characteristic signature for the Au substrate.

Electron reflectivity spectra from substrates with immobilized reduced dithiol-modified oligonucleotides are shown in Fig. 16 (center and bottom). The reflectivity data were derived by averaging the intensity over a square, $1\,\mu m \times 1\,\mu m$ area near the center of a DNA island as well as from uncoated areas on the Au substrate, while the landing energy is increased in 0.1 eV steps. The electron reflectivity spectra from uncoated areas on the Au substrate provide reference spectra that can be used to compare spectra from different DNA oligonucleotides deposited on separate Au substrates.

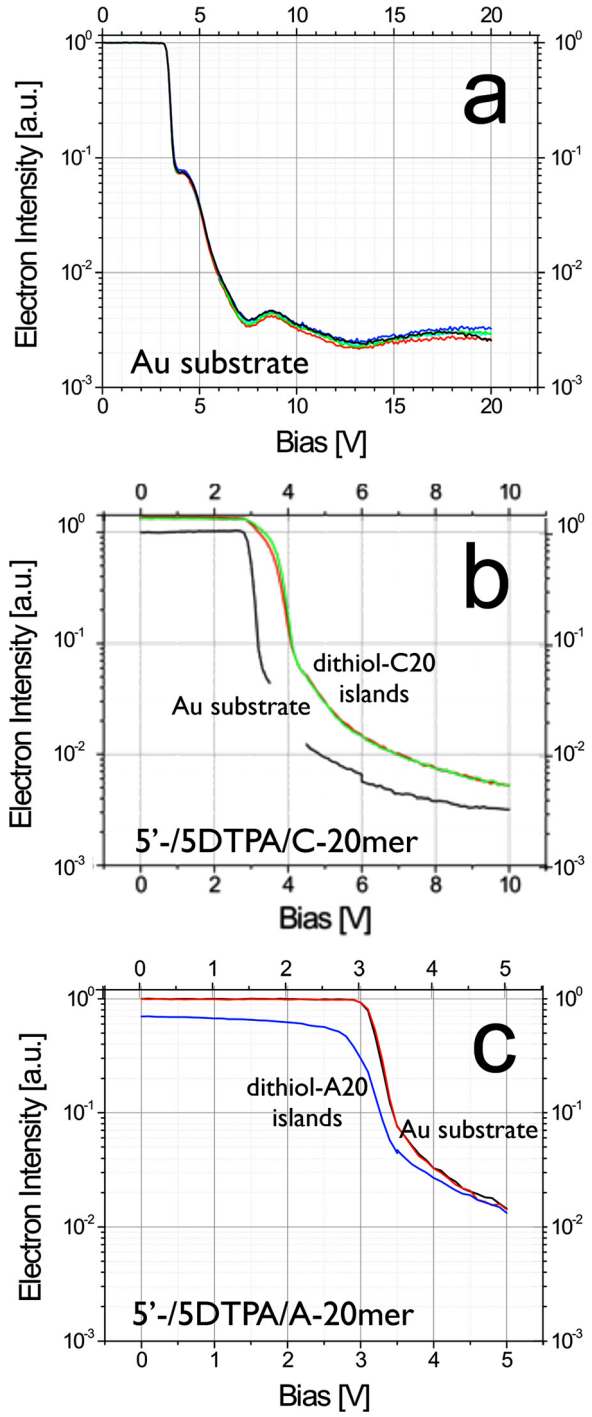

FIG. 16. (Color online) Electron reflectivity spectra from clean Au substrates (a), Au substrates with immobilized reduced 5′-/5DTPA/C-20mers (b) and 5′-/5DTPA/A-20mers (c).

Early results indicate that immobilized islands with different bases (5′-/5DTPA/C-20mers versus 5′-/5DTPA/A-20mers) produce different "signatures" when compared to the underlying Au layer and thus hold promise for distinguishing individual nucleotides without labels. The electron reflectivity curves in Fig. 16 show two distinct features: a shift in work function and contrast reversal of the two types of oligonucleotides with respect to the Au substrate. At a landing energy of 5 eV, the C20mer islands show strong

bright contrast (more than 3 × the signal compared to the Au surface), while the A20mer island reflectivity is close to that of the Au substrate at this landing energy. This should result in rather large contrast between A20mer and C20mer islands. While these initial results are promising, more experimental data are needed to quantify the contrast and verify that the contrast obtained on bulk samples will be preserved on the nanoscale of the DNA strand. More experimental work is planned in the coming year in order to better understand the dependence of the contrast on landing energy and optical blur.

V. SUMMARY AND CONCLUSIONS

The electron–optical concept of MAD-LEEM, a novel microscopy technique utilizing a monochromator, aberration corrector, and dual-beam electron illumination, has been presented. The imaging principles of the key components have been reviewed, and a detailed approach for DNA sequencing has been proposed. A novel monochromator design utilizes an electron mirror that reduces the energy spread of the illuminating electron beam, which significantly improves spectroscopic and spatial resolution. Simulations of electron–optical properties of the LEEM objective lens have been completed including aberrations up to 5th order in order to understand the resolution limit with aberration correction. Analysis of electrostatic electron mirrors shows that their negative spherical and chromatic aberration coefficients can be tuned over a large parameter range and used to compensate the aberrations of the LEEM objective lens for a range of electron energies. A novel mirror aberration corrector, an electrostatic pentode mirror, combined with the monochromator has been proposed to further improve the resolution by correcting the 5th order spherical aberration. With this correction, the spatial resolution may be reduced to less than 1 nm for landing energies ranging from tens of eV to a few hundred eV. An electron–optical design combining a monochromator with an aberration corrector and capable of delivering two parallel electron beams with different energies and beam currents at the specimen surface has been devised.

Experimental images of thin DNA structures immobilized on a gold substrate obtained in a LEEM demonstrate that high contrast is achievable at low electron energies in the range of 1–10 eV, a prerequisite for our approach. Electron reflectivity measurements derived from these LEEM images over a range of landing energies show that small changes in landing energy have a strong impact on the DNA contrast and thus in combination with the theoretical results on aberration correction hold promise for distinguishing individual nucleotides without labels.

Simulations of the MAD-LEEM electron optics show that subnanometer resolution can be achieved by incorporating a Pentode MAC and a monochromator. This approach thus has promise to significantly improve the performance of a LEEM for a wide range of applications in the biosciences, material sciences, and nanotechnology where nanometer scale resolution and analytical capabilities are required. The objective is to establish a sufficient level of confidence to justify an experimental machine to be developed.

ACKNOWLEDGMENTS

The authors would like to thank T.H.P. Chang for his continuous support and numerous suggestions leading to this paper. They would also like to thank Eric Munro and John Rouse of MEBS Ltd. (London, UK) for their support and fruitful discussions. This project was supported by Grant Number R43HG006303 from the National Human Genome Research Institute (NHGRI). The content is solely the responsibility of the authors and does not necessarily represent the official views of the NHGRI or the National Institutes of Health. LEEM imaging was performed at the National Center for Electron Microscopy, Lawrence Berkeley National Laboratory, and was supported by the Office of Science, Office of Basic Energy Sciences, Scientific User Facilities Division, of the U.S. Department of Energy under Contract No. DE-AC02—05CH11231. A.T.N. acknowledges support from the Alexander von Humboldt Foundation.

[1]W. Telieps and E. Bauer, Ultramicroscopy **17**, 57 (1985).
[2]M. S. Altman, J. Phys.: Condens. Matter **22**, 084017 (2010).
[3]H. Hibino H. Kageshima, F. Maeda, M. Nagase, Y. Kobayashi, Y. Kobayashi, and H. Yamaguchi, e-J. Surf. Sci. Nanotechol. **6**, 107 (2008).
[4]M. Mankos, V. Spasov, and E. Munro, in *Advances in Imaging and Electron Physics*, edited by P. W. Hawkes (Elsevier Ltd., 2010), Vol. 161, p. 1.
[5]M. Mankos, H. F. Hess, D. L. Adler, and K. J. Bertsche, U.S. patent 6,870,172 (22 March 2005).
[6]O. L. Krivanek, J. P. Ursin, N. J. Bacon, G. J. Corbin, N. Dellby, P. Hrncirik, M. F. Murfitt, C. S. Own, and Z. S. Szilagyi, Phil. Trans. R. Soc. A **367**, 1 (2009).
[7]H. H. Rose, Sci. Technol. Adv. Mater. **9**, 014107 (2008).
[8]H. W. Mook and P. Kruit, Ultramicroscopy **81**, 129 (2000).
[9]M. Mankos, U.S. patent 8,870,172 (22 May 2012).
[10]Electron Optica MG6000, "Monochromatic thermal-field emission gun," see: www.electronoptica.com.
[11]O. Scherzer, Z. Phys. **101**, 593 (1936).
[12]M. Haider, H. Rose, S. Uhlemann, B. Kabius, and K. Urban, J. Electron. Microsc. **47**, 395 (1998).
[13]O. L. Krivanek, N. Dellby, and A. R. Lupini, Ultramicroscopy **78**, 1 (1999).
[14]G. F. Rempfer and M. S. Mauck, Optik **92**, 3 (1992).
[15]Th. Schmidt *et al.*, Ultramicroscopy **110**, 1358 (2010).
[16]R. M. Tromp, J. B. Hannon, A. W. Ellis, W. Wan, A. Berghaus, and O. Schaff, Ultramicroscopy **110**, 852 (2010).
[17]D. Preikszas and H. Rose, J. Electron Microsc. **1**, 1 (1997).
[18]Th. Schmidt *et al.*, Surf. Rev. Lett. **9**, 223 (2002).
[19]M. Mankos, A. Sagle, S. T. Coyle, and A. Fernandez, J. Vac. Sci. Technol. B **19**, 467 (2001).
[20]R. M. Tromp, W. Wan, and S. M. Schramm, Ultramicroscopy **110**, 333 (2012).
[21]E. Munro, J. Rouse, H. Liu, and L. Wang, J. Vac. Sci. Technol. B **26**, 2331 (2008).
[22]W. Wan, J. Feng, H. A. Padmore, and D. S. Robin, Nucl. Instrum. Meth. Phys. Res. A **519**, 222 (2004).
[23]H. Rose and D. Krahl, in *Energy-Filtering Transmission Electron Microscopy*, edited by L. Reimer, Springer Series in Optical Sciences (Springer-Verlag, 1995), Vol. 71, pp. 43–149.
[24]M. Mankos, D. Adler, L. Veneklasen, and E. Munro, Surf. Sci. **601**, 4733 (2007).
[25]L. H. Veneklasen and D. L. Adler, U.S. patent 6,803,572 (12 October 2004).
[26]M. Mankos, Nucl. Instrum. Meth. Phys. Res. A **645**, 35 (2011).
[27]J. D. Watson and F. Crick, Nature **171**, 737 (1953).
[28]W. R. Glover III, U.S. patent 7,288,379 (30 October 2007).
[29]W. Andregg and M. Andregg, U.S. Patent Application No. 20100267152 (21 October 2010).

[30]M. Germann, T. Latychevskaia, C. Escher, and H.-W. Fink, Phys. Rev. Lett. **104**, 095501 (2010).
[31]S. Kilina, S. Tretiak, D. A. Yarotski, J. Zhu, N. Modine, A. Taylor, and A. V. Balatsky, J. Phys. Chem. C **111**, 14541 (2007).
[32]R. G. Endres, D. L. Cox, and R. R. P. Singh, Rev. Mod. Phys. **76**, 195 (2004).
[33]X. Guo, A. A. Gorodetsky, J. Hone, J. K. Barton, and C. Nuckolls, Nat. Nanotechnol. **3**, 163 (2008).
[34]A. Bensimon, A. Simon, A. Chiffaudel, V. Croquette, F. Heslot, and D. Bensimon, Science **265**, 2096 (1994).
[35]See: http://www.nanoink.net/pdf/DataSheets/Substrates/DS_Substrate_MicaPeeledGold.pdf.